Robust Subthermionic Topological Transistor Action via Antiferromagnetic Exchange

Sagnik Banerjee, Koustav Jana, Anirban Basak, Michael S. Fuhrer, Dimitrie Culcer, and Bhaskaran Muralidharan

Phys. Rev. Applied **18**, 054088 — Published 29 November 2022

DOI: 10.1103/PhysRevApplied.18.054088

Robust Subthermionic Topological Transistor Action via Antiferromagnetic Exchange

Sagnik Banerjee,[1,*] Koustav Jana,[2,*] Anirban Basak,[2] Michael S. Fuhrer,[3,4] Dimitrie Culcer,[5,6] and Bhaskaran Muralidharan[2,7,†]

[1] *Department of Electronics and Telecommunication Engineering, Jadavpur University, Jadavpur-700032, India*
[2] *Department of Electrical Engineering, Indian Institute of Technology Bombay, Powai, Mumbai-400076, India*
[3] *School of Physics and Astronomy, Monash University, Clayton, Victoria 3800, Australia*
[4] *ARC Centre of Excellence in Future Low-Energy Electronics Technologies (FLEET), Monash University, Clayton, Victoria 3800, Australia*
[5] *School of Physics, University of New South Wales, Sydney 2052, Australia*
[6] *ARC Centre of Excellence in Future Low-Energy Electronics Technologies (FLEET), University of New South Wales, Sydney 2052, Australia*
[7] *Center of Excellence in Quantum Information, Computation, Science and Technology, Indian Institute of Technology Bombay, Powai, Mumbai-400076, India*

The topological quantum field-effect transition in buckled 2D-Xenes can potentially enable subthermionic transistor operation coupled with a dissipationless ON-state conduction. We investigate realistic device structures which exploit the quantum field effect transition between the dissipationless topological phase and the band insulator phase. We find that the previously considered dual-gate structure is disadvantageous, leading to a near-doubling of the subthreshold swing. However, we identify a single-gate strategy capable of overcoming the thermionic limit at the cost of sacrificing the dissipationless ON-state conduction. By introducing an out-of-plane antiferromagnetic exchange in the material via proximity coupling we exploit transitions between the quantum spin-valley Hall and the spin quantum anomalous Hall phase, which restore the topological robustness of the ON state while simultaneously surpassing the thermionic limit. Our work thus outlines a realistic pathway to topological transistors that can overcome Boltzmann's tyranny while preserving topological robustness.

I. INTRODUCTION

A fundamental challenge today in the evolution of field-effect transistors (FETs) is the compulsory power penalty resulting from a fundamental thermionic limit, also known as Boltzmann's tyranny. This relates to the steepness of the transfer characteristics: the subthreshold swing (SS) [1–3], which is conventionally restricted to 60mV/dec at room temperature. In the context of low-power devices, it is hence paramount to innovate strategies to suppress the SS, thereby ensuring a sub-thermionic operation. Several attempts have been made to overcome this limit, popular ones include tunnel FETs [4–6], impact ionization MOSFETs [7] and negative capacitance FETs (NC-FETs) [8–16], to name a few. While the aforementioned paradigms are typically based on transitions between the insulating and the conducting phase, this work aims to investigate realistic device structures that exploit transitions between the dissipationless topological insulator (TI) phase and the trivial band insulator (BI) phase.

The SS quantifies the corresponding change in drain current I_D due to a change in gate voltage V_G and is given by the expression $(d[logI_D]/dV_G)^{-1}$. One can further segment the expression into two terms, i.e. $d[logI_D]/dV_G = (d[logI_D]/d\psi) \times (d\psi/dV_G)$ by invoking the surface potential ψ which relates to the position of the channel bandstructure with respect to the Fermi level. The first term, $d[logI_D]/d\psi$, depends on the carrier transport mechanism in the subthreshold regime. The value of this term is limited to $k_B T ln(10)/q$, because of thermionic emission-based carrier transport in conventional FETs. This limit can be surpassed by the use of tunnel FETs (TFETs) where carrier transport is based on band-to-band tunneling [4–6]. Although TFETs enable subthermionic operation, their ON-state current is significantly compromised due to tunneling-based transport, which gives less current when compared to the drift current in conventional transistors.

On the other hand, the second term, $d\psi/dV_G$, is dependent on the electrostatic design of the transistor and is at best ≈ 1 in the ideal case of complete gate control over the channel. In this context, there has been a lot of interest in the use of ferroelectric materials to endow a negative capacitance (NC) in the transistor gate stack [8–16]. As a result, NC-FETs can achieve $d\psi/dV_G > 1$ and attain SS below the Boltzmann's limit. However, there are certain challenges to be addressed because of the energetic instability in the NC regime of ferroelectric insulators [17].

Looking ahead, it is also possible to engineer $d\psi/dV_G$ to be greater than unity via a faster-than-linear translation of the bandgap with the topological phase transition between TI phase (ON state) and the trivial BI phase (OFF state) [18–23] in 2D TIs. This can be achieved via the inclusion of an electric field-dependent Rashba spin-orbit interaction [18], which can be termed as the topological quantum field-effect (TQFE). The TQFE adds to the electrostatic field-effect from the gates, potentially

* These authors contributed equally
† bm@ee.iitb.ac.in

propelling a steeper SS [18]. One can thus envision a topological quantum field-effect transistor (TQFET) built to harness the TQFE.

Combining the steep-subthreshold slope performance with the dissipationless edge modes in the TI phase makes TQFETs excellent prospects for futuristic low-power electronics. A great deal of experimental effort has thus already been geared towards the realization of topological transistors [24–27]. Quantum spin Hall (QSH) materials such as group-IV and V-Xenes with buckled 2D honeycomb lattices [21, 22, 28–32], monolayer transition metal dichalcogenides in the 1T' configuration [33], HgTe nanoribbons [34] and thin films of 3D topological insulators Bi_2Se_3 [35, 36] as well as Dirac semi-metals like Na_3Bi [37] are among the prominent material candidates.

The demonstration of a workable device design uniting the merits of a dissipationless channel along with the possibility of overcoming Boltzmann's tyranny using the TQFE [18] can thus underline the operational criteria for designing TQFETs as a building block for low-power electronics. In this work, we present such a framework for a holistic analysis of TQFETs and highlight the engineering intricacies involved in harnessing the Rashba spin orbit interaction (SOI) for a steep SS, while simultaneously preserving the topological robustness of the ON state. Building on this, we propose a device structure that utilizes the spin quantum anomalous Hall (SQAH) state induced via an out-of-plane antiferromagnetic (AF) exchange to achieve the desired performance.

Furthermore, employing the Keldysh non-equilibrium Green's function (NEGF) formalism [41–43], we uncover fundamental sub-threshold limits posed by the gating mechanism that effectuates such a transition. By presenting an in-depth analysis of the band translations necessitated by the field effect, we demonstrate that the thermionic limit of the SS in the TQFETs, designed according to conventional principles, is half as steep as that of the conventional FETs i.e., $k_B T \ln(10)/q$ [18]. In an attempt to alleviate this issue, we propose to engineer the gate biasing to modulate one of the bands while restricting the other, ultimately attaining an SS transcending the thermionic limit of 60 mV/dec at room temperature. However, this also introduces dissipative conduction modes from the bulk in the ON state, defeating one of the desired attributes in a TQFET. As a tactical solution, we demonstrate that the introduction of out-of-plane antiferromagnetic exchange interaction, which can be induced via proximity coupling [44] restores the dissipationless ON state and can effectively harness the Rashba-assisted TQFET.

II. FORMULATION

All the transport calculations are based on the Keldysh NEGF formalism [41–43, 45], within the tight binding framework of the model Hamiltonian, well described in various works, which we will briefly describe [19, 20, 23, 46].

A. Device Hamiltonian

The building block of the TQFET is a 2D TI with a buckled honeycomb lattice structure that forms the channel as depicted in Fig. 1(a). For numerical calculations pertinent to our proposed topological transistor, we consider the typical tight-binding Hamiltonian model for the 2D buckled honeycomb lattice [47, 48] in the second quantized notation:

$$\hat{H} = -t \sum_{\langle i,j\rangle\alpha} c^{\dagger}_{i\alpha} c_{j\alpha} + i\frac{\lambda_{SO}}{3\sqrt{3}} \sum_{\langle\langle i,j\rangle\rangle\alpha\beta} \nu_{ij} c^{\dagger}_{i\alpha} s^{z}_{\alpha\beta} c_{j\beta} + \lambda_v \sum_{i\alpha} c^{\dagger}_{i\alpha} \mu_i c_{i\alpha} + i\lambda_R \sum_{\langle ij\rangle\alpha\beta} c^{\dagger}_{i\alpha} (s_{\alpha\beta} \times \hat{d}_{ij})_z c_{j\beta}, \quad (1)$$

where $c^{(\dagger)}_{i\alpha}$ represents the electronic annihilation (creation) operator on site i with a spin $\alpha = \uparrow (\downarrow)$, and $\langle i,j\rangle$ and $\langle\langle i,j\rangle\rangle$ characterize the nearest neighbour and the next-nearest neighbour hopping respectively. The spin indices are represented with corresponding values $+1/-1$ respectively. The first term in (1) represents the nearest-neighbor hopping term with a hopping strength t. The second term represents the intrinsic spin-orbit (SO) coupling with strength λ_{SO}, where $\nu_{ij} = +1(-1)$ for anti-clockwise (clockwise) next-nearest neighbour hopping with respect to the positive z-axis. The third term denotes the staggered sub-lattice potential of strength λ_v, with $\mu_i = +1(-1)$, where i denotes the sub-lattice A(B). The fourth term represents the nearest neighbour Rashba spin-mixing interaction, with $s_{\alpha\beta}$ denoting the corresponding matrix elements indicating spin-polarization α, β at lattice sites i, j respectively, and $\hat{d}_{ij}$ is the distance vector between lattice sites i and j.

B. Calculation of the transmission coefficient

The I-V characteristics are calculated from the energy resolved transmission coefficient $T(E)$, which is evaluated using the Green's function as:

$$T(E) = \mathbf{Tr}[\Gamma_L(E) G^R(E) \Gamma_R(E) G^A(E)] \quad (2)$$

$$[\Gamma_{L,R}(E)] = i[\Sigma_{L,R}(E) - \Sigma_{L,R}(E)^{\dagger}] \quad (3)$$

$$[G^R(E)] = [(E + i\eta)I - H - \Sigma_L(E) - \Sigma_R(E)]^{-1} \quad (4)$$

where $\mathbf{Tr}$ represents the trace operation, $[\Gamma_{L(R)}(E)]$ is the broadening matrix corresponding to the lead $L(R)$, and $[G^R(E)]$ and $[G^A(E)]$ are the matrix representations

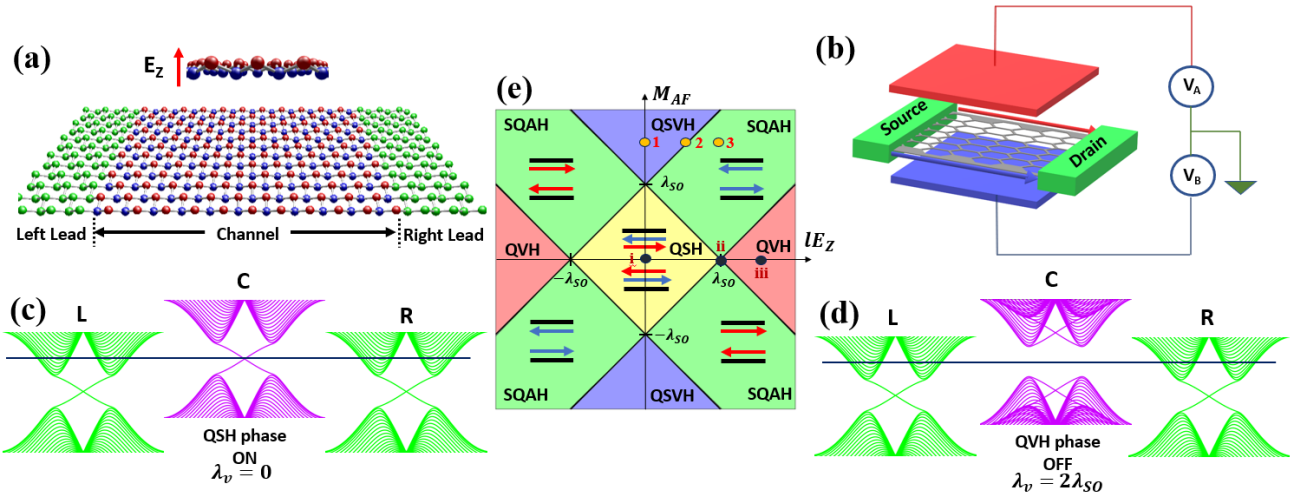

Figure 1. Device structure and phase transitions. **a)** A 2D buckled honeycomb monolayer Xene is used as the channel (C), left (L), and right (R) lead material. The leads are colored green to distinguish them from the channel region, where the two sub-lattices A(B) are represented in red and blue respectively. **b)** Schematic representation of a dual-gated device structure. The top and bottom gates have applied potentials V_A and V_B respectively so that the net potential difference across the channel material is $(V_A - V_B)$. For the symmetric bias arrangement, $V_A = \lambda_v/2$ and $V_B = -\lambda_v/2$. **c, d)** Band structures of the channel and leads for the TQFET, in the ON and the OFF-state respectively. The Fermi level (E_f) is represented by a solid black line. **e)** Phase diagram of a monolayer Xene nanoribbon with homogeneous perpendicular electric field and antiferromagnetic exchange field [38–40].

of the retarded and advanced Green's functions respectively. All quantities in the above equations can be obtained from the Hamiltonian defined in (1) and the self-energy matrices $[\Sigma_{L,R}]$, which are calculated recursively based on the formalism prescribed in [45, 46].

Finally, the current calculations are performed based on the Landauer transmission formula, with the transmission coefficient evaluated from the device retarded Green's function

$$I = \frac{e^2}{h}\int_{-\infty}^{\infty} T(E)(f(E,\mu_L,T) - f(E,\mu_R,T))dE, \quad (5)$$

where $f(E,\mu,T) = (1 + exp(\frac{E-\mu}{k_B T}))^{-1}$ is the Fermi-Dirac distribution at Fermi energy μ and temperature T. The impressed voltage across the device is given as $qV = \mu_L - \mu_R$, where $\mu_{L(R)}$ represents the Fermi energy of the left (right) lead.

III. RESULTS AND DISCUSSION

In the transistor setup depicted in Fig. 1(b), an electric field (E_Z) applied perpendicular to the buckled lattice manifests as a staggered potential between the sub-lattice A and B of the honeycomb unit cell. The dual-gate structure helps in realizing the electric field between the two plates, hence imparting a capacitive action. Such a dual-gate manifestation of a topological transistor also enables a two-fold biasing scheme: a) symmetric biasing, where equal and opposite bias voltages are applied to the two gates, i.e., $V_A = -V_B$, and b) rigid biasing, where the entire voltage is applied to one of the gate plates with the other plate grounded. For the symmetric bias setup the Fermi level is positioned as in Fig 1(c) and Fig 1(d) to ensure topological ON state conduction.

It is worth remarking at this point that we have primarily focused on group-IV and V Xenes with buckled honeycomb lattice. The buckled structure possessed by these materials allows us to manipulate their topological nature by means of a perpendicular electric field created using a dual-gate structure. Also the inclusion of additional effects like Rashba SOI and antiferromagnetic exchange, critical for our device design, can be modeled very conveniently by adding extra terms to the channel Hamiltonian, as discussed in the subsequent sections. It is also worth mentioning that more innovative and advanced spin-orbit materials like 1T'MoS_2 could also be a potential candidate for the channel material. However, incorporating such materials as the channel would demand investigation into the effect of Rashba SOI and antiferromagnetic exchange on the Hamiltonian from first-principle calculations. Also, these materials have a more complicated lattice structure than group-IV and V Xenes and hence, a detailed study of electric field-induced topological quantum field-effect is needed for such materials.

Previous proposals of topological transistors using buckled Xene nanoribbons have been mostly based on the QSH-QVH phase transition on varying the out-of-plane electric field, which effectively navigates the horizontal axis of the phase diagram, as depicted by the points i, ii and iii in Fig. 1(e). Apart from the above, one can have new topological phases on the inclusion of

an out-of-plane antiferromagnetic (AF) exchange field, represented by the vertical axis in Fig. 1(e). Navigating along the horizontal direction for an AF exchange greater than some critical value, as depicted by the points 1, 2 and 3 in Fig. 1(e), one can have a topological transition between an insulating quantum spin valley Hall (QSVH) phase and a conducting spin quantum anomalous Hall (SQAH) phase [38–40]. In the SQAH phase the AF interaction breaks the time reversal symmetry (TRS), resulting in spin-polarized conducting modes without a chiral counter-propagating partner.

To analytically investigate the subthreshold physics of topological transistors, we adopt the low energy effective four-band Bloch Hamiltonian H_η in the vicinity of Dirac points $K(K')$ as given by (6). This Dirac Hamiltonian has been derived from the tight-binding Hamiltonian model described in (1) for the 2D buckled honeycomb lattice [21, 22, 47, 48].

$$H_\eta = \hbar v_f(\eta k_x\tau_x + k_y\tau_y)\sigma_0 + \eta\lambda_{SO}\tau_z\sigma_z + \lambda_v\left(E_Z\right)\tau_z\sigma_0 + \frac{\lambda_R\left(E_Z\right)}{2}(\eta\tau_x\sigma_y - \tau_y\sigma_x), \quad (6)$$

where $\eta = +(-)$ is the valley index denoting $K(K')$ and, σ and τ are the spin and pseudo-spin Pauli matrices respectively. Here, $\hbar$ is the reduced Planck's constant and v_f denotes the Fermi velocity, given by the expression $v_f = 3ta_o/2$ where t is the hopping parameter and a_o is the lattice constant. The quantities λ_{SO}, λ_v and λ_R denote the strengths of the intrinsic spin-orbit coupling, staggered sublattice potential and Rashba spin-mixing interaction respectively.

In the context of an electric field induced topological phase transition between the QVH and the QSH phases [46], it is important to analyze the Chern number [23] ($\mathcal{C}$) and the nature of the edge states. For $\lambda_v < \lambda_{SO}$, the QSH phase is characterized by a zero total Chern number $\mathcal{C}$ and a non-zero spin Chern number $2\mathcal{C}_s = +2$ resulting in helical edge states as illustrated in Fig. 2(a). A phase transition at $\lambda_v = \lambda_{SO}$, as in Fig. 2(b), results in the QVH phase for $\lambda_v > \lambda_{SO}$. This band insulator phase is characterized by both zero $\mathcal{C}$ and $2\mathcal{C}_s$, leading to a trivial gap as shown in Fig. 2(c). The faster closing and reopening of gap for the $\lambda_R \neq 0$ case when compared to $\lambda_R = 0$ case, as shown in Fig. 2, nicely illustrates the topological quantum field effect (TQFE) switching.

The total current with components I_c and I_v due to the electrons in the conduction band (CB) and holes in the valence band (VB) is given as

$$I_c = I_{co}\exp-\frac{q\left(E_c - E_f\right)}{k_BT}$$
$$I_v = I_{vo}\exp\frac{q\left(E_v - E_f\right)}{k_BT}, \quad (7)$$

where $I_{co(vo)}$ is the CB (VB) current maximum, $E_{c(v)}$ represents the CB (VB) minimum (maximum), and E_f denotes the equilibrium Fermi energy level. Here, k_BT is the thermal energy at temperature T.

The SS of a transistor during the ON-OFF state transition is defined as

$$SS = \left|\frac{d(log_{10}I)}{dV_G}\right|^{-1}, \quad (8)$$

where $I\ (= I_c + I_v)$ represents the current in response to an applied gate voltage V_G. Substituting I from (7) in (8), we get,

$$SS = \frac{k_BT}{q}ln(10)\frac{I}{\left|I_v\left(\frac{dE_v}{dV_G}\right) - I_c\left(\frac{dE_c}{dV_G}\right)\right|}, \quad (9)$$

where $k_BTln(10)/q$ is the thermionic limit at temperature T, which reduces to 60 mV/decade at room temperature. We then define S^*, which is the reduced SS [18] as,

$$S^* = \frac{I}{\left|I_v\left(\frac{dE_v}{dV_G}\right) - I_c\left(\frac{dE_c}{dV_G}\right)\right|}. \quad (10)$$

For conventional MOSFETs, it has hitherto been assumed that $S^* \geq 1$. Moreover, it is anticipated in [18] that the introduction of Rashba interactions can achieve $S^* \leq 1$ to overcome the Boltzmann's limit. However, we now demonstrate that this limit (S^*) for a TQFT is, unfavorably, twice as much.

Figure 3(a) depicts the n-MOS operation of a conventional transistor. For an applied gate bias ΔV_G, both the CB and the VB move equally by an amount proportional to ΔV_G. For an n-MOS device, this upward ascent of the bands results in $I_c \gg I_v$. In this case, both (dE_c/dV_G) and (dE_v/dV_G) are unity since both bands translate by an equal amount ($\propto \Delta V_G$).

For a TQFET with $\lambda_R = 0$, however, the translation of bands in response to ΔV_G is non-trivial. As depicted in Fig. 3(b), both the bands move away from the Fermi level by an amount proportional to $\Delta V_G/2$ in the OFF state. So, $(dE_c/dV_G) = 1/2$ and $(dE_v/dV_G) = -1/2$ for a TQFET with $\lambda_R = 0$. Moreover, due to symmetry in the band translation, the current components $I_c \approx I_v \approx I/2$. This results in $S^* \approx 2$ and hence the SS in a standard TQFET will be restricted to $2k_BTln(10)/q$ instead of $k_BTln(10)/q$. At room temperature, this translates to the thermionic limit being restricted to 120 mV/decade instead of 60 mV/decade in the conventional case.

With the introduction of the Rashba SOI term, the band translation during the OFF state (QVH phase) is asymmetric. From the Dirac Hamiltonian elaborated in (6), we calculate E_c and E_v for $\lambda_v > \lambda_{SO} > 0$, i.e., in the OFF state as follows:

$$E_v = \lambda_{SO} - \lambda_v$$
$$E_c = -\lambda_{SO} + \sqrt{\lambda_v^2 + \lambda_R^2}, \quad (11)$$

where, λ_v and λ_R can be represented as $\alpha_V E_Z$ and $\alpha_R E_Z$ respectively since they are both linearly proportional to the gate electric field E_Z. Taking derivatives

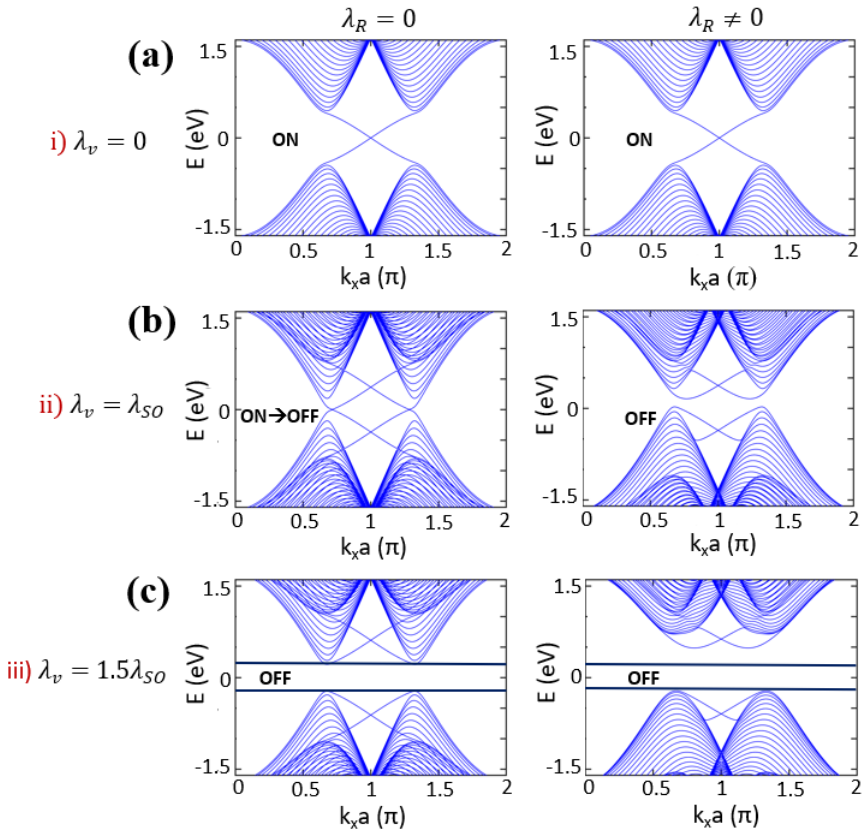

Figure 2. Band structures of the channel for different λ_v. **a)** The QSH phase characterized by topologically protected edge states. Here, we have assumed $\lambda_v = 0$ and considered two cases of $\lambda_R = 0$ and $\lambda_R \neq 0$. **b)** depicts the transition from QSH to QVH phase for the $\lambda_R = 0$ case. For the $\lambda_R \neq 0$ case, the system has already entered the band insulator phase. Here, we have considered $\lambda_v = \lambda_{SO}$, where λ_{SO} is the intrinsic spin-orbit coupling strength. **c)** demonstrates a faster retreat of the CB in the $\lambda_R \neq 0$ case compared to the $\lambda_R = 0$ case. The VB in both cases remains almost pinned. Here, $\lambda_v = 1.5\lambda_{SO}$.

with respect to V_G we get, $(dE_v/dV_G) = -1/2$ and $(dE_c/dV_G) = 0.5\sqrt{(1+\alpha_R^2/\alpha_V^2)}$. Note that, putting $\alpha_R = 0$ we get same results as estimated previously for the $\lambda_R = 0$ case. Also, we notice that in the QVH phase, the CB translates faster with increasing gate bias than the VB due to the effect of the Rashba term α_R. However, since $|E_v| < |E_c|$, we expect I_v to contribute more to the current than I_c. Thus, from (10) we expect (dE_v/dV_G) to contribute more to the SS. Thus, the improved SS due to (dE_c/dV_G) is undone by the relatively smaller contribution from I_c. This mechanism has been represented schematically in Fig. 3(c).

In Fig. 3(d), we show the evaluated subthreshold characteristics using the NEGF approach [41–43, 45]. We set $T = 300$K and $\lambda_{SO} = 0.41$eV with a hopping parameter $t = 1.6$eV, consistent with first-principles calculations [18]. We assume a finite-sized nanoribbon as the channel material, with a device length $N_L = 45$ and width $N_W = 20$. The NEGF simulations reconcile with the analytical conclusions drawn. Despite the introduction of Rashba interactions, the SS is limited to $2k_B T\ln(10)/q$ or 120 mV/decade at $T = 300$K. With the symmetric gate biasing, as seen in previous sections, the channel Fermi level is pinned in the middle of the bandgap of the channel. As a result, in the QVH phase (OFF) the channel conducts the smallest possible current. Moreover, using symmetric gate biasing, the SS cannot be improved significantly below 120mV/dec even in the presence of Rashba SOI. Hence, an alternate approach is required which relies upon a smart positioning of the channel Fermi level to create an imbalance in the rate with which the two bands move away from the channel Fermi level, as a function of the applied gate voltage.

The easiest way to do this would be via an asymmetric gate biasing where V_A and V_B corresponding to Fig. 1(b) are set to V_G and zero respectively. This particular gating scheme has an added advantage that it is compatible with the modern-day transistor architectures because of it requiring only a single gate voltage as opposed to the dual gate voltage requirement of symmetric gate biasing. Now positioning the Fermi level at $E = 0$ (solid line in Fig. 4(a-d)) leads to an immanent problem as described below. At $\lambda_v = 0$, as shown in Fig. 4(a), the Fermi level lies right at the middle of the bandgap. Because of rigid biasing in the QSH phase, only the VB moves with varying gate voltage and after a certain point, the Fermi

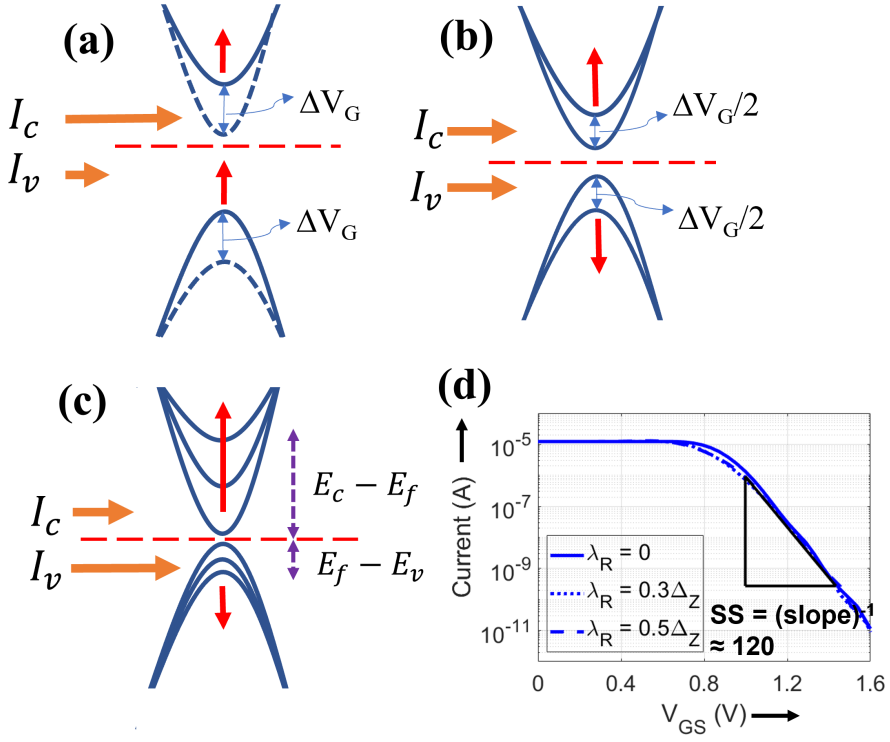

Figure 3. Band translation schematics and I-V characteristics for QSH-QVH transition based FET. **a)** represents the band movement in an ordinary n-MOSFET for an applied bias potential of ΔV_G. Here, $I_C > I_V$ **b)** represents the band movement in the OFF state of a topological transistor with $\lambda_R = 0$. Here, $I_C = I_V$. **c)** represents the band movement in the OFF state of a topological transistor with $\lambda_R \neq 0$. Here, $I_C < I_V$. **d)** is the I-V characteristics of a topological transistor based upon phase transition from ON ($V_G < 0.8$V) to OFF ($V_G > 0.9$V) phase, for different Rashba strengths of $\lambda_R = 0$, $\lambda_R = 0.3\Delta_Z$ and $\lambda_R = 0.5\Delta_Z$. Here, $\Delta_Z = \lambda_v$. For all the three cases, the subthreshold-swing (SS) remains confined to 120 mV/decade of current.

level slips inside the VB. Beyond the critical field, the Fermi level remains pinned inside the VB. As a result, the TQFET does not turn OFF in the QVH phase, because of the VB bulk states participating in the conduction. Despite the Fermi level in the leads being aligned to the CB, leakage current conduction in the OFF state may be facilitated by band-to-band tunneling as depicted in Fig. 4(e), which is undesirable. (Note that in ideal operation, the device does not rely on any band-to-band tunneling effects.)

The problem highlighted above arises because of the Fermi level lying inside the VB in the QVH phase resulting in a deteriorated OFF state. One obvious way to alleviate this issue is to align the Fermi level inside the bandgap for the QVH phase. However, in this scenario, the Fermi level moves inside the CB in the QSH phase (ON state). Thus, apart from the dissipationless edge modes, even the dissipative bulk states participate in conduction. This strategy restores the full advantage of the Rashba SOI-enabled TQFE in reducing the SS. However, conduction no longer occurs solely through dissipationless edge states. This may be disadvantageous, though the details of the ON state conduction will depend on material and device parameters, and in principle dissipative bulk states can also contribute to enhanced ON current. Thus, by allowing dissipative bulk state conduction, it is possible to achieve subthermionic performance with negligible OFF current, by aligning the Fermi level as shown by the dashed lines in Fig. 4(a-d).

The obtained I-V characteristics for the above case are as shown in Fig. 4(f). The ON current is significantly higher ($> 10^4$) when compared to that of the symmetric biasing case in Fig. 3(d), owing to the fact that the current-carrying states in the ON state are now the bulk modes of the QSH phase. Because of rigid gate biasing, as illustrated by our numerical simulations, the SS calculated for $\lambda_R = 0$ is around 60mV/dec, the thermionic limit at 300K. The inclusion of Rashba SOI further enhances the subthreshold performance with SS values of 52mV/dec and 50mV/dec for the cases of $\lambda_R = 0.3\Delta_z$

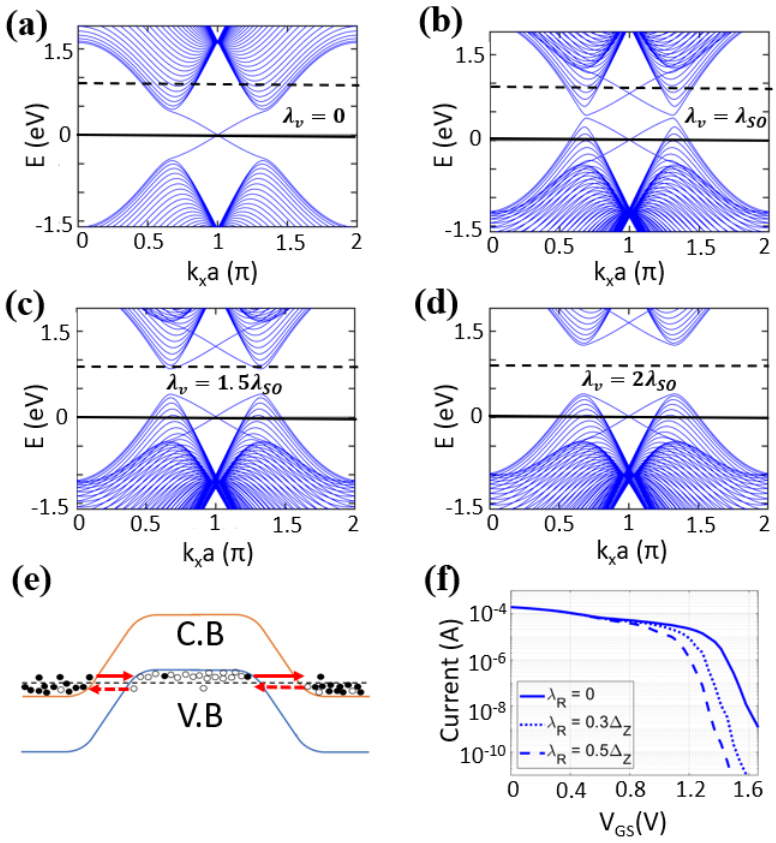

Figure 4. Rigid biasing approach wherein $V_A = V_G$ and $V_B = 0$. The band structures for varying λ_v along with the corresponding Fermi levels (elaborated in text) are depicted in **(a-d)**. **(e)** illustrates the possible band-to-band tunneling when the channel Fermi level lies inside the VB, leading to undesirable OFF current. **(f)** is the I-V characteristics for a rigidly biased TQFET with suitably positioned Fermi level for different values of λ_R. The corresponding SS values for $\lambda_R = 0$, $0.3\Delta_z$, and $0.5\Delta_z$ are 60mV/dec, 52mV/dec, and 49mV/dec respectively

and $0.5\Delta_z$ respectively, thus exemplifying subthermionic performance enabled by the introduction of Rashba SOI for a rigidly biased TQFET with a suitably positioned Fermi level.

While the above strategy is a robust route to a subthermionic transistor, we would also like to understand whether it is possible to retain both the subthermionic SS and the dissipationless edge transport in the ON state. Dissipationless edge transport should provide significant advantages for certain device geometries and hence, is an indispensable feature to retain. We thus explore ideas beyond the QSH-QVH transition and look into new topological phases. As suggested by (9), one way to achieve $S^* \leq 1$ is by ensuring that at least one of the quantities (dE_c/dV_G) and (dE_v/dV_G) exceeds unity. If, say, the CB satisfies this, then for subthermionic performance the CB current should be the major contributor of the total current. In other words, we can attain subthermionic performance by ensuring $(dE_c/dV_G) \geq 1$ and $I_c \gg I_v$.

In the QSH-QVH transition-based TQFET with symmetric biasing, evident from (11), it is possible to achieve $(dE_c/dV_G) \geq 1$ in the presence of a large enough Rashba SOI. However as a result of this, in the QVH phase, the CB moves away from the Fermi level at a greater rate than the VB and we get $I_v \gg I_c$, as illustrated in Fig. 3(c), and thus there is no discernible improvement in S^*. This happens because in the OFF state the bandgap opens as we increase the gate voltage. For the Rashba influenced band to contribute more to the total current, the bandgap should close as the applied field increases. In such a scenario, the Rashba influenced band would be closer to the Fermi level throughout the subthreshold regime (OFF state). This will eventually lead to a subthermionic performance.

The above scenario can be realized by the addition of AF exchange interaction, which can be incorporated via proximity coupling [44] to a 2D topological insulator implying the addition of the term $M_{AF}\tau_z\sigma_z$ to the low-energy Hamiltonian in (6). As represented by the points (1),(2) and (3) in Fig. 1(e), for $M_{AF} > \lambda_{SO}$, one can realize the QSVH phase and the SQAH phases by varying the perpendicular electric field [38–40]. For $\lambda_v < M_{AF} - \lambda_{SO}$, we obtain the QSVH phase with a Chern number $\mathcal{C} = 0$ and no gapless edge states. On the other hand, $\lambda_v > M_{AF} - \lambda_{SO}$ opens the SQAH phase with a Chern number $\mathcal{C} = 1$, possessing spin-polarized

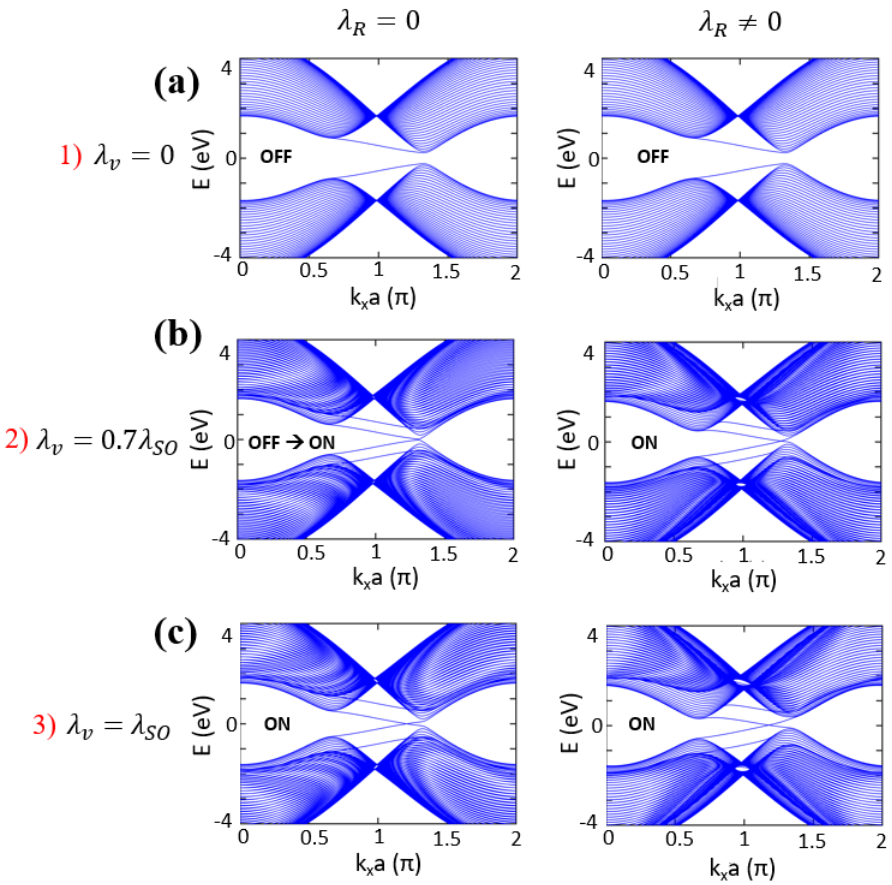

Figure 5. Band structures of the channel for different λ_v highlights the underlying switching principle under the influence of an antiferromagnetic term. **a)** represents the quantum spin valley Hall (QSVH) phase characterized by an insulating gap for the two valleys K(K'). Here, we have assumed $\lambda_v = 0$ and considered two cases of $\lambda_R = 0$ and $\lambda_R \neq 0$. **b)** depicts the QSVH-SQAH transition for the $\lambda_R = 0$ case. For the $\lambda_R \neq 0$ case, topologically protected edge states are prominent. Here, we have considered $\lambda_v = 0.5\lambda_{SO}$, λ_{SO} being the intrinsic spin-orbit coupling strength. **c)** demonstrates the onset of ON phase for both the $\lambda_R = 0$ and $\lambda_R \neq 0$ case. Here, we have chosen $\lambda_v = 0.8\lambda_{SO}$.

chiral edge states. The perfect spin polarization of the edge currents may also provide connections to spintronics applications. Here, the QSVH phase represents the OFF state, i.e., the transition is from OFF to ON as the gate voltage increases, contrary to the scenario in the QSH-QVH transition.

Now, as depicted in Fig. 6(a), the bandgap closes in the subthreshold regime on increasing gate voltage and the Rashba influenced VB moves closer to the Fermi level, such that $I_v \gg I_c$. In this case, if λ_R is large enough for dE_v/dV_G to be greater than unity, it is possible to achieve $S^* < 1$. Analytically, based on the low-energy Dirac Hamiltonian in (6), and in presence of Rashba SOI, we have the following in the QSVH phase:

$$\begin{aligned} E_v &= \lambda_{SO} - M_{AF} + \sqrt{\lambda_v^2 + \lambda_R^2} \\ E_c &= M_{AF} - \lambda_{SO} - \lambda_v. \end{aligned} \tag{12}$$

Clearly, on increasing E_z, the VB approaches the Fermi level at a greater rate for a non-zero λ_R, and the VB current is the major contributor.

These analytical findings are well supported by the simulated results in Fig. 6(b). Here the following parameters are considered: $\lambda_{SO} = 0.41eV$, $M_{AF} = 1.7\lambda_{SO}$. We consider three values of λ_R for comparison: $\lambda_R = 0$, $0.5\Delta_z$ and $0.8\Delta_z$, where $\Delta_z = \lambda_v$. The $\lambda_R = 0$ case, similar to the previous QSH-QVH case, gives an SS of around 120mV/dec, because of symmetric band translation under symmetric biasing. However, upon increasing λ_R, we notice a significant improvement in the SS, with the topological transistor achieving $SS < 60$mV/dec for $\lambda_R = 0.8\Delta_z$. Thus the addition of an out-of-plane AF exchange interaction to a 2D-TQFET under symmetric biasing can attain subthermionic characteristics. One thing to note is that the current remains constant in the ON state for an appreciable range of gate voltage, suggesting that the dissipationless edge modes are responsible for the ON state conduction. Adding to this, a TQFET hosting chiral QAH edge modes is expected to be more resilient to back-scattering than the one having helical QSH edge modes. This is because QSH requires the time-reversal symmetry (TRS) to be preserved for maintain-

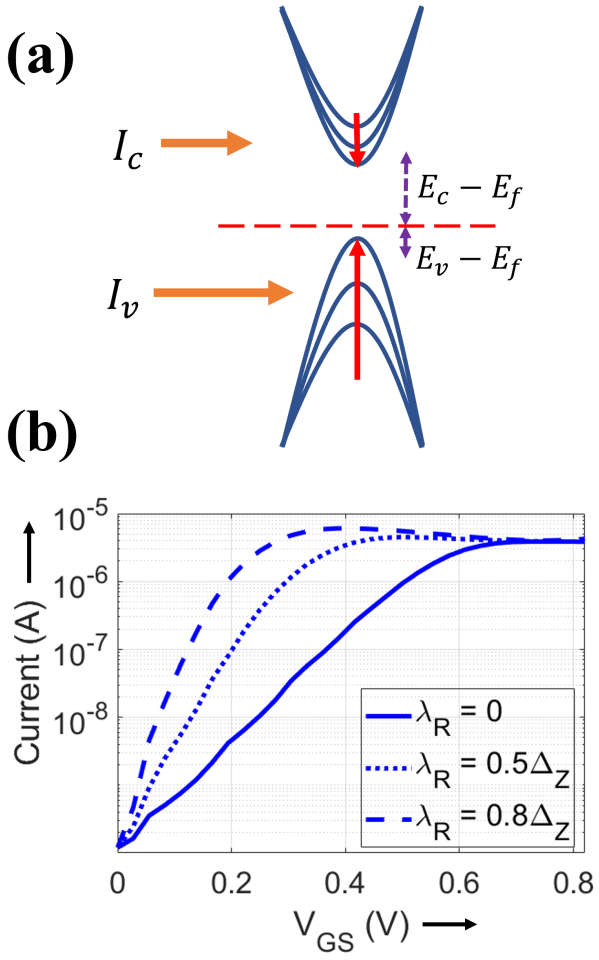

Figure 6. Transistor operation with the inclusion of the AF interaction. **a)** The band translation schematics in the OFF state of a TQFET is when $I_C < I_V$. The Fermi level is closer to the VB than the CB. **b)** The I-V characteristics based on phase transitions in the subthreshold region for different Rashba interactions, for $\Delta_Z = \lambda_v$. We notice a progressive improvement in the SS as λ_R increases.

ing its robustness. However, this is not the case with the QAH phase which is robust even to back-scattering by magnetic disorder, because of the absence of any time-reversal partner for the chiral edge modes.

IV. CONCLUSION

This work dealt with an in-depth analysis of how a topological field effect transition can effectuate a sub-thermionic transistor operation. We investigated realistic device structures which exploit the quantum field effect transition between the dissipationless topological phase and the band insulator phase. Our analysis revealed that the previously considered dual-gate structure is disadvantageous, leading to a near-doubling of the subthreshold swing. However, we identified a single-gate strategy capable of beating the thermionic limit at the cost of sacrificing the dissipationless ON-state conduction. By introducing an out-of-plane antiferromagnetic exchange in the material via proximity coupling we demonstrated how to exploit transitions between the QSVH and the SQAH phase, which restores the topological robustness of the ON state while simultaneously surpassing the thermionic limit. Our work thus outlines a realistic pathway to topological transistors that can overcome the Boltzmann's tyranny while preserving the topological robustness. Further analysis along the lines of introducing defects and the study of dephasing [46, 49] and their effects on the topological robustness is a fruitful direction to move the analysis forward. Future works that develop electro-thermal transport [50], as well as high-frequency analysis [51–53] in order to concretize the transistor operation is necessary to realize the goal of topological electronics [24]-the engineering of emerging devices from topological quantum matter.

ACKNOWLEDGEMENTS

The author BM wishes to acknowledge the Visvesvaraya Ph.D Scheme of the Ministry of Electronics and Information Technology (MEITY), Government of India, implemented by Digital India Corporation (formerly Media Lab Asia). The author BM also wishes to acknowledge the support by the Science and Engineering Research Board (SERB), Government of India, Grant No. Grant No. STR/2019/000030, and the Ministry of Human Resource Development (MHRD), Government of India, Grant No. STARS/APR2019/NS/226/FS under the STARS scheme. Authors MSF and DC acknowledge the support from the ARC Centre of Excellence in Future Low-Energy Electronics Technologies (CE170100039).

[1] MS Lundstrom. The mosfet revisited: device physics and modeling at the nanoscale. In *2006 IEEE international SOI Conferencee Proceedings*, pages 1–3. IEEE, 2006.

[2] Takayasu Sakurai. Perspectives of low-power vlsi's. *IEICE transactions on electronics*, 87(4):429–436, 2004.

[3] Deblina Sarkar, Xuejun Xie, Wei Liu, Wei Cao, Jiahao Kang, Yongji Gong, Stephan Kraemer, Pulickel M Ajayan, and Kaustav Banerjee. A subthermionic tunnel field-effect transistor with an atomically thin channel. *Nature*, 526(7571):91–95, 2015.

[4] Masaharu Kobayashi. A perspective on steep-subthreshold-slope negative-capacitance field-effect transistor. *Applied Physics Express*, 11(11):110101, 2018.

[5] DM Newns, JA Misewich, CC Tsuei, A Gupta, BA Scott, and A Schrott. Mott transition field effect transistor. *Applied Physics Letters*, 73(6):780–782, 1998.

[6] Sanjay K Banerjee, Leonard F Register, Emanuel Tutuc, Dharmendar Reddy, and Allan H MacDonald. Bilayer pseudospin field-effect transistor (bisfet): A proposed new logic device. *IEEE Electron Device Letters*, 30(2):158–160, 2008.

[7] Kailash Gopalakrishnan, Peter B Griffin, and James D Plummer. Impact ionization mos (i-mos)-part i: device and circuit simulations. *IEEE Transactions on electron devices*, 52(1):69–76, 2004.

[8] Sayeef Salahuddin and Supriyo Datta. Use of negative capacitance to provide voltage amplification for low power nanoscale devices. *Nano Letters*, 8(2):405–410, 2008.

[9] Jorge Íñiguez, Pavlo Zubko, Igor Luk'yanchuk, and Andrés Cano. Ferroelectric negative capacitance. *Nature Reviews Materials*, 4(4):243–256, 2019.

[10] Alexandru Rusu, Giovanni A Salvatore, David Jimenez, and Adrian M Ionescu. Metal-ferroelectric-meta-oxide-semiconductor field effect transistor with sub-60mv/decade subthreshold swing and internal voltage amplification. In *2010 international electron devices meeting*, pages 16–3. IEEE, 2010.

[11] Zoran Krivokapic, U Rana, R Galatage, A Razavieh, A Aziz, J Liu, J Shi, HJ Kim, R Sporer, C Serrao, et al. 14nm ferroelectric finfet technology with steep subthreshold slope for ultra low power applications. In *2017 IEEE International Electron Devices Meeting (IEDM)*, pages 15–1. IEEE, 2017.

[12] Ali Saeidi, Farzan Jazaeri, Francesco Bellando, Igor Stolichnov, Gia V Luong, Qing-Tai Zhao, Siegfried Mantl, Christian C Enz, and Adrian M Ionescu. Negative capacitance as performance booster for tunnel fets and mosfets: an experimental study. *IEEE electron device letters*, 38(10):1485–1488, 2017.

[13] Mengwei Si, Chun-Jung Su, Chunsheng Jiang, Nathan J Conrad, Hong Zhou, Kerry D Maize, Gang Qiu, Chien-Ting Wu, Ali Shakouri, Muhammad A Alam, et al. Steep-slope hysteresis-free negative capacitance mos 2 transistors. *Nature nanotechnology*, 13(1):24–28, 2018.

[14] Xiaowei Wang, Peng Yu, Zhendong Lei, Chao Zhu, Xun Cao, Fucai Liu, Lu You, Qingsheng Zeng, Ya Deng, Jiadong Zhou, et al. Van der waals negative capacitance transistors. *Nature communications*, 10(1):1–8, 2019.

[15] Felicia A McGuire, Yuh-Chen Lin, Katherine Price, G Bruce Rayner, Sourabh Khandelwal, Sayeef Salahuddin, and Aaron D Franklin. Sustained sub-60 mv/decade switching via the negative capacitance effect in mos2 transistors. *Nano letters*, 17(8):4801–4806, 2017.

[16] Michael S. Fuhrer, Mark T. Edmonds, Dimitrie Culcer, Muhammad Nadeem, Xiaolin Wang, Nikhil Medhekar, Yuefeng Yin, and Jared H Cole. Proposal for a negative capacitance topological quantum field-effect transistor. *ArXiv: 2201.05288*, 2022.

[17] Wei Cao and Kaustav Banerjee. Is negative capacitance FET a steep-slope logic switch? *Nature Communications*, 11(1):196, January 2020.

[18] Muhammad Nadeem, Iolanda Di Bernardo, Xiaolin Wang, Michael S Fuhrer, and Dimitrie Culcer. Overcoming boltzmann's tyranny in a transistor via the topological quantum field effect. *Nano Letters*, 21(7):3155–3161, 2021.

[19] Motohiko Ezawa. Electrically tunable conductance and edge modes in topological crystalline insulator thin films: minimal tight-binding model analysis. *New Journal of Physics*, 16(6):065015, 2014.

[20] Motohiko Ezawa. Quantized conductance and field-effect topological quantum transistor in silicene nanoribbons. *Applied Physics Letters*, 102(17):172103, 2013.

[21] Motohiko Ezawa. Monolayer topological insulators: Silicene, germanene, and stanene. *J. Phys. Soc. Japan*, 84(12):121003, 2015.

[22] Motohiko Ezawa. Valley-polarized metals and quantum anomalous hall effect in silicene. *Phys. Rev. Lett.*, 109:055502, Aug 2012.

[23] Koustav Jana and Bhaskaran Muralidharan. Robust all-electrical topological valley filtering using monolayer 2d-xenes. *npj 2D Materials and Applications*, 6(1):19, Mar 2022.

[24] Matthew J Gilbert. Topological electronics. *Communications Physics*, 4(1):1–12, 2021.

[25] Jifa Tian, Cuizu Chang, Helin Cao, Ke He, Xucun Ma, Qikun Xue, and Yong P Chen. Quantum and classical magnetoresistance in ambipolar topological insulator transistors with gate-tunable bulk and surface conduction. *Scientific reports*, 4(1):1–10, 2014.

[26] Hao Zhu, Curt A Richter, Erhai Zhao, John E Bonevich, William A Kimes, Hyuk-Jae Jang, Hui Yuan, Haitao Li,

Abbas Arab, Oleg Kirillov, et al. Topological insulator bi 2 se 3 nanowire high performance field-effect transistors. *Scientific reports*, 3(1):1–5, 2013.

[27] Han Liu and Peide D Ye. Atomic-layer-deposited al2o3 on bi2te3 for topological insulator field-effect transistors. *Applied Physics Letters*, 99(5):052108, 2011.

[28] Hongki Min, JE Hill, Nikolas A Sinitsyn, BR Sahu, Leonard Kleinman, and Allan H MacDonald. Intrinsic and rashba spin-orbit interactions in graphene sheets. *Physical Review B*, 74(16):165310, 2006.

[29] Cheng-Cheng Liu, Wanxiang Feng, and Yugui Yao. Quantum spin hall effect in silicene and two-dimensional germanium. *Physical review letters*, 107(7):076802, 2011.

[30] Yong Xu, Binghai Yan, Hai-Jun Zhang, Jing Wang, Gang Xu, Peizhe Tang, Wenhui Duan, and Shou-Cheng Zhang. Large-gap quantum spin hall insulators in tin films. *Physical review letters*, 111(13):136804, 2013.

[31] Chia-Hsiu Hsu, Zhi-Quan Huang, Feng-Chuan Chuang, Chien-Cheng Kuo, Yu-Tzu Liu, Hsin Lin, and Arun Bansil. The nontrivial electronic structure of bi/sb honeycombs on sic (0001). *New Journal of Physics*, 17(2):025005, 2015.

[32] F Reis, G Li, L Dudy, M Bauernfeind, S Glass, W Hanke, R Thomale, J Schäfer, and R Claessen. Bismuthene on a sic substrate: A candidate for a high-temperature quantum spin hall material. *Science*, 357(6348):287–290, 2017.

[33] Xiaofeng Qian, Junwei Liu, Liang Fu, and Ju Li. Quantum spin hall effect in two-dimensional transition metal dichalcogenides. *Science*, 346(6215):1344–1347, 2014.

[34] Hua-Hua Fu, Jin-Hua Gao, and Kai-Lun Yao. Topological field-effect quantum transistors in hgte nanoribbons. *Nanotechnology*, 25(22):225201, 2014.

[35] Wen-Yu Shan, Hai-Zhou Lu, and Shun-Qing Shen. Effective continuous model for surface states and thin films of three-dimensional topological insulators. *New Journal of Physics*, 12(4):043048, 2010.

[36] Chao-Xing Liu, HaiJun Zhang, Binghai Yan, Xiao-Liang Qi, Thomas Frauenheim, Xi Dai, Zhong Fang, and Shou-Cheng Zhang. Oscillatory crossover from two-dimensional to three-dimensional topological insulators. *Physical review B*, 81(4):041307, 2010.

[37] James L Collins, Anton Tadich, Weikang Wu, Lidia C Gomes, Joao NB Rodrigues, Chang Liu, Jack Hellerstedt, Hyejin Ryu, Shujie Tang, Sung-Kwan Mo, et al. Electric-field-tuned topological phase transition in ultrathin na 3 bi. *Nature*, 564(7736):390–394, 2018.

[38] Yafang Xu and Guojun Jin. Manipulating topological inner-edge states in hybrid silicene nanoribbons. *Phys. Rev. B*, 95:155425, Apr 2017.

[39] Chun-Xia Zhang, Xiao-Long Lü, and Hang Xie. Spin and spin-valley filter analysis of inner-edge states in hybrid silicene-like nanoribbons. *Journal of Physics D: Applied Physics*, 53(19):195302, mar 2020.

[40] Motohiko Ezawa. Spin valleytronics in silicene: Quantum spin hall–quantum anomalous hall insulators and single-valley semimetals. *Phys. Rev. B*, 87:155415, Apr 2013.

[41] Supriyo Datta. *Electronic transport in mesoscopic systems*. Cambridge university press, 1997.

[42] Yigal Meir and Ned S Wingreen. Landauer formula for the current through an interacting electron region. *Physical review letters*, 68(16):2512, 1992.

[43] Hartmut Haug, Antti-Pekka Jauho, et al. *Quantum kinetics in transport and optics of semiconductors*, volume 2. Springer, 2008.

[44] Semonti Bhattacharyya, Golrokh Akhgar, Matthew Gebert, Julie Karel, Mark T Edmonds, and Michael S Fuhrer. Recent progress in proximity coupling of magnetism to topological insulators. *Advanced Materials*, 33(33):2007795, 2021.

[45] Supriyo Datta. *Lessons from Nanoelectronics*. World Scientific, 2nd edition, 2018.

[46] Anirban Basak, Pratik Brahma, and Bhaskaran Muralidharan. Momentum relaxation effects in 2d-xene field effect device structures. *Journal of Physics D: Applied Physics*, 55(7):075302, nov 2021.

[47] Charles L Kane and Eugene J Mele. Z 2 topological order and the quantum spin hall effect. *Physical review letters*, 95(14):146802, 2005.

[48] Charles L Kane and Eugene J Mele. Quantum spin hall effect in graphene. *Physical review letters*, 95(22):226801, 2005.

[49] Aritra Lahiri, Kaveh Gharavi, Jonathan Baugh, and Bhaskaran Muralidharan. Nonequilibrium green's function study of magnetoconductance features and oscillations in clean and disordered nanowires. *Phys. Rev. B*, 98:125417, Sep 2018.

[50] Aniket Singha and Bhaskaran Muralidharan. Performance analysis of nanostructured peltier coolers. *Journal of Applied Physics*, 124(14):144901, 2018.

[51] Andrii Iurov, Godfrey Gumbs, and Danhong Huang. Temperature- and frequency-dependent optical and transport conductivities in doped buckled honeycomb lattices. *Phys. Rev. B*, 98:075414, Aug 2018.

[52] Andrii Iurov, Godfrey Gumbs, Danhong Huang, and Ganesh Balakrishnan. Thermal plasmons controlled by different thermal-convolution paths in tunable extrinsic dirac structures. *Phys. Rev. B*, 96:245403, Dec 2017.

[53] Sukhwinder Singh, Kartikey Thakar, Naveen Kaushik, Bhaskaran Muralidharan, and Saurabh Lodha. Performance projections for two-dimensional materials in radio-frequency applications. *Phys. Rev. Applied*, 10:014022, Jul 2018.